

Review

Abrasion Evaluation of Moon and Mars Simulants on Rotating Shaft/Sealing Materials: Simulants and Structural Materials Review and Selection

György Barkó¹, Gábor Kalácska¹ , Róbert Keresztes¹, László Zsidai¹, Hailemariam Shegawu¹ and Ádám Kalácska^{2,*}

¹ Institute of Technology, Szent István Campus, Magyar Agrár- és Élettudományi Egyetem (MATE), Páter Károly u. 1, 2100 Gödöllő, Hungary; barko.gyorgy.csaba@uni-mate.hu (G.B.)

² Soete Laboratory, Department of Electromechanical, Systems and Metal Engineering, Ghent University, Technologiepark 46, B-9052 Zwijnaarde, Belgium

* Correspondence: adam.kalacska@ugent.be

Abstract: Tribological testing of moving shaft/sealing pairs in complex environments is at the frontline of research. Machines working in abrasive conditions are subject to different wear effects. It is not only valid on Earth but especially valid for rovers and future robots used in Mars and Moon missions. The aim of our joint research with the European Space Agency is to study the abrasion phenomena of moving machine elements on Mars and the Moon by using artificial soil samples (“simulants”). This review details mainly the available simulant sources and recommend a selection of the most suitable ones for tribological testing. Moreover, the potential mating structural materials subjected to abrasive space applications are reviewed briefly. The tribological tests are exploring the features of the rotary shaft/seal relationship that is subject to dry friction and intense abrasion. By using the simulants, measurements are performed under laboratory conditions with both a sample test and a real shaft/seal connection. Parameters of the selection criteria were defined, and classification of the simulant sources were made. It was found that simulant particle size distribution and chemical substance content are detailed enough only for a limited type of available artificial Moon and Mars soil samples. Four simulants were identified and applied later in the tribological testing. For the shaft materials, based on a detailed case study of polymers, steel, and aluminum alloys, a high-strength aluminum alloy with a hard anodized surface and a stainless steel were selected for further abrasion tests.

Keywords: Mars simulant; moon simulant; rotary shaft; sealings



Citation: Barkó, G.; Kalácska, G.; Keresztes, R.; Zsidai, L.; Shegawu, H.; Kalácska, Á. Abrasion Evaluation of Moon and Mars Simulants on Rotating Shaft/Sealing Materials: Simulants and Structural Materials Review and Selection. *Lubricants* **2023**, *11*, 334. <https://doi.org/10.3390/lubricants11080334>

Received: 14 June 2023
Revised: 16 July 2023
Accepted: 24 July 2023
Published: 7 August 2023



Copyright: © 2023 by the authors. Licensee MDPI, Basel, Switzerland. This article is an open access article distributed under the terms and conditions of the Creative Commons Attribution (CC BY) license (<https://creativecommons.org/licenses/by/4.0/>).

1. Introduction

The application of regolith simulants in test laboratories is general practice [1]. These artificial regolith samples prepared are similar to those found on planetary surfaces. Thanks to the lander and rover missions sent to explore Mars, details are available on the substance composition of the soil at different sites across the planet. Two of the earliest Martian missions, the Viking I and II landers, scrape away at the top few centimeters of the regolith surrounding the landing sites (Table 1).

The Mars mission ‘Pathfinder’ successfully landed on the Martian surface in 1997, deploying the Sojourner rover. This mission demonstrated the feasibility of traversing the Martian regolith and provided additional information about it. Sojourner also performed the wheel abrasion experiment and utilized it to profile the abrasiveness of the regolith particles and give information about the shapes of the particles. Subsequently, the Mars Exploration Rover (MER) missions utilized the first optical microscopes on Mars. Rovers were equipped also with spectrometers, providing real composition data from a huge range of sites. Lander missions to Mars, InSight and Phoenix, extended the results originating

from the Viking missions. The thermal and evolved gas analyzer on the landers profiled the substances in the regolith further. Additionally, the trenches left by the rover scoop action provided information about the mechanical properties of the soil.

Table 1. Constitution of Mars surface soil [2].

Composition	Viking Lander I—Surface Soil (wt%)
SiO ₂	43
FeO	0
Fe ₂ O ₃	18.5
Al ₂ O ₃	7.3
SO ₃	6.6
MgO	6.0
CaO	5.9
Others/not identified	12.7

There is a renewed interest in exploring the Moon, leading to upcoming missions by various space agencies, including the U.S., Russia, China, Japan, the EU, and Canada [3]. A lunar regolith simulant is required to develop rover missions that can successfully explore the surface of the Moon. These regolith simulants shall accurately represent the soils that exist on the Moon's surface. Several high-fidelity simulants are available based on chemical substance content, particle size distribution, and particle shape. These artificial regolith products are offered to test different applications. Simple simulants used the fine fraction of ground granular basalts with surface weathering. Advanced simulants utilized state-of-the-art technology to closely approach the original regolith composition and substance content/ratio as well as the electrostatic behavior.

Newson et al. [3] characterized the geomechanical performance of various simulants. The outcomes of the mechanical property tests revealed that the simulants exhibit comparable mechanical responses to angular and rough soils, and their behavior closely aligns with that of two widely recognized geotechnical benchmark soils, establishing their reliability and applicability in geotechnical studies.

The preparation of Moon or Mars soil simulants and selecting raw materials for an artificial regolith is challenging. The experimental process shall ensure that the Earth-based raw materials used in these processes are comparable in their physical and mechanical properties to those observed on the Moon or Mars. Specifications for internal friction angle and cohesion can be utilized as general mechanical parameters. Particle size distribution, dry bulk density, and particle shape must be considered as well. For geomechanical testing, the high fidelity of the chemical substance content/ratio is not a priority for the selection of simulants.

This paper provides a collection of potential Mars and Moon simulants, compares them based on chemical composition and size distribution, and provides recommendation for the selection of the most suitable simulants for tribological testing. Additionally, the commonly used shaft and sealing materials subjected to abrasive conditions in space are analyzed and reviewed.

2. Materials

2.1. Review on the Preparation of Martian and Lunar Abrasive Simulants

Martian simulants have been prepared by Böttger et al. [4]. Simulants were used to specifically test a Raman laser spectrometer on the ExoMars rover and its ability to identify organics and minerals. They were meant to represent the environmental change on Mars from early hydrothermal alteration to later cold and dry oxidizing conditions. The materials were crushed and mixed, then sieved to a <1 mm size fraction for experiments. The components are described in Table 2.

Table 2. Mineralogical composition of phyllosilicatic Mars regolith simulant (P-MRS) and sulfatic Mars regolith simulant (S-MRS) [4].

Component	P-MRS (wt%)	S-MRS (wt%)
Gabbro	3	32
Olivine	2	15
Quartz	10	3
Hematite	5	13
Montmorillonite	45	-
Chamosite	20	-
Kaolinite	5	-
Siderite	5	-
Hydromagnesite	5	-
Goethite	-	7
Gypsum	-	30

A specific simulant, “JSC”, was developed by Allen et al. [5]. JSC Mars-1 was prepared for scientific research and for engineering tests and academic purposes. JSC Mars-1 is the <1 mm fraction of weathered volcanic ash from Pu’u Nene, which is a residue of the cone on the island of Hawaii. Pu’u Nene ash has also been selected based on its spectral similarity to material located on bright regions of Mars. This kind of simulant is available in significant quantity. Chemical composition compared with Viking landers (VL-1 and VL-2) and Pathfinder composition data (Table 3) and grain size distribution are shown in Table 4.

Table 3. Pathfinder data about chemical composition [5].

Oxide	VL-1	WL-2	Pathfinder	JSC Mars-1	
	Wt%	Wt%	Wt%	Wt%	Wt%
SiO ₂	43	43	44.0	34.5	43.5
Al ₂ O ₃	7.3	7	7.5	18.5	23.3
TiO ₂	0.66	0.56	1.1	3.0	3.8
Fe ₂ O ₃	18.5	17.8	16.5	12.4	15.6
MnO	n.a.	n.a.	n.a.	0.2	0.3
CaO	5.9	5.7	5.6	4.9	6.2
MgO	6	6	7.0	2.7	3.4
K ₂ O	<0.15	<0.15	0.3	0.5	0.6
Na ₂ O	n.a.	n.a.	2.1	1.9	2.4
P ₂ O ₅	n.a.	n.a.	n.a.	0.7	0.9
SO ₃	6.6	8.1	4.9	n.a.	n.a.
Cl	0.7	0.5	0.5	n.a.	n.a.
LOI	n.a.	n.a.	n.a.	21.8	n.a.
Total	89	89	89.5	101.1	100.0

Table 4. Grain size distribution [5].

Size (µm)	Wt%
450–1000	21
250–449	30
150–249	24
53–149	19
5–52	5
<5	1

Another widely used simulant was developed by Cannon et al. [6]. The paper describes the Mars Global Simulant (MGS-1), a high-fidelity mineralogical representative of basaltic regolith on Mars. The prototype simulant was utilized to characterize basic physical,

chemical, and spectral properties and volatile content. MGS-1 has been applied to test Mars rovers and remote sensing equipment. This kind of simulant is produced in large amounts by the Center for Lunar and Asteroid Surface Science (CLASS) Exolith Lab, and it is commercially available. By publishing the mineral recipe and production methods, authors anticipate that other groups can recreate the simulant and modify it as they see fit, leading to a more sustainable model for simulant production and the possibility of extending the simulant for different regions on Mars or different applications.

An analogue approach was used by Exolith Lab to prepare the Jezero crater simulant. The Jezero Delta Simulant (JEZ-1) was made to simulate materials in the Jezero crater deltas. This is the geographical area that is investigated by the NASA Mars 2020 rover mission. Based on orbital remote sensing of Jezero delta deposits, JEZ-1 is a mixture of MGS-1 composition with smectite clay, magnesium carbonate, and olivine. Due to potential mineralogical deviations, limitations in simulant fidelity must be considered.

Soil sample extraction tests, excavation, or rover mobility evaluation requires a significant amount of simulant up to a couple of hundred kilograms. High-fidelity simulants are expensive and not available in such order of magnitude to fill in the rover test bed. Low-fidelity simulants have been proven to be a reasonable trade-off and applicable to these tests. However, test results must be carefully calculated, and geotechnical properties reported in detail, allowing for repeating the experiments in a relevant test environment. This process step is missed in several excavation studies reported.

A low-fidelity but large-scale lunar simulant was made and evaluated by Just et al. [7]. Large-scale engineering experiments involving excavation, sampling, and mobility in rocky planetary surface exploration, such as on the Moon, frequently demand extensive test beds filled with significant quantities of soil, often amounting to hundreds of kilograms. However, specially engineered regolith simulants are expensive and may not be available in sufficient quantities due to limited production rates. As a result, the use of low-fidelity analogues becomes a practical alternative. Nevertheless, it is crucial to report the geotechnical properties of these analogues to accurately calculate excavation and traction forces and ensure the comparability and repeatability of results. Unfortunately, this vital step of characterizing the analogues is often overlooked in studies focusing on regolith handling and excavation.

Two low-fidelity simulants, UoM-B and UoM-W, have been identified as potential candidates for large-scale simulant test bed experiments. Both geotechnical characteristics (particle morphology, particle size distribution, specific gravity, maximum and minimum densities, and shear strength parameters) and chemical substance content have been investigated. Results acquired have been relevant to values of other available Moon regolith simulants, as well as features of Apollo regolith samples. However, the chemical contents of UoM-B and UoM-W are different from the Moon regolith obtained during Apollo missions; both simulants demonstrated meaningful similarity from a mechanical property standpoint that allows us to apply them for low-fidelity but large-scale experiments. Linke et al. [8] dedicated efforts to develop Lunar Mare and Lunar Highlands Simulants. TUBS-M = Mare; TUBS-T = Highlands simulants originated from basaltic and anorthositic bedrock. The aim was to match the two dominant lunar surface rock types. In terms of raw material sources, TUBS-M has been prepared from an alkali-olivine basalt in Germany. The material for manufacturing TUBS-T originated from a Scandinavian metamorphosed gabbroic complex. The production process of the two simulants has been described. Their characteristics in terms of mineralogy (Table 5), chemical composition (Table 6), and physical properties (Table 7) are presented. Figure 1 (self-made picture) shows the mentioned simulants.

Table 5. Mineralogy [8].

Component	TUBS-M (Wt%)	TUBS-T (Wt%)
Basalt	100	0
Anorthosite	0	100

Table 6. Bulk chemistry [8].

Oxide	TUBS-M (Wt%)	TUBS-T (Wt%)
SiO ₂	48.61	48.71
TiO ₂	2.29	0.12
Al ₂ O ₃	13.28	30.33
FeO>	10.14	1.05
MgO	8.73	0.57
CaO	8.31	14.57
Na ₂ O	3.67	3.05
K ₂ O	1.71	0.22
MnO	0.18	0.015
Cr ₂ O ₃	0.04	0.00

Table 7. Physical properties [8].

Property	TUBS-M	TUBS-T
Grain density	2.96 g/cm ³	2.71 g/cm ³
Bulk density	1.41 g/cm ³	1.18 g/cm ³
Angle of repose	41.9–45.8°	37.91°
Particle size range	0–2.0 mm	0–2.0 mm
Median	87 μm	87 μm
Cohesion	0.6 kPa	1.46 kPa

**Figure 1.** TUBS-M and TUBS-T lunar regolith simulants.

A wide range of large amounts of lunar simulants and additives are offered by the enterprise Off Planet Research [9]. Two major simulants offered are Archean anorthosite (Source: Shawmere Anorthosite Complex, Foleyet, ON, Canada) and basaltic cinder (Source: San Francisco Formation near Flagstaff in AZ, USA). Archean anorthosite is mineralogically similar to the lunar mineral form. Anorthosite originated from Foleyet, ON, Canada was primary feedstock source in preparing Lunar Highlands simulants. Anorthosites from this source have been proven to be unaltered from the original state. Basaltic cinder north to Flagstaff, Arizona is mineralogically comparable to Lunar Mare low-titanium basalt regolith and has high glass content, which supports its use as a simulant for basaltic regolith. Several added components are offered as well, including material: ilmenite (titanium- and iron-based mineral, standard concentration = 14.4%), agglutinates, iron and iron dioxide, and silica dioxide. The company offers several customized mixtures made from the materials above. The LMS-1 Lunar Mare Simulant was developed by the CLASS Exolith Lab, Oviedo, FL, USA [10]. It is a high-fidelity, mineral-based simulant appropriate for a generic or average mare location on the Moon. The simulant is not made of a single terrestrial lithology but accurately captures the texture of lunar regolith by combining both mineral and rock fragments (i.e., polyminerale grains) in accurate proportions. The particle size distribution of the simulant is targeted to match that of typical Apollo soils. Physical properties are summarized below.

- Mean particle size: 50 μm
- Median particle size: 45 μm
- Particle size range: <0.04–300 μm
- Uncompressed bulk density: 1.56 g/cm^3

At present, LMS-1 does not replicate the characteristics of agglutinates or nanophase iron in its composition. The mineralogical table (Table 8) summarizes the properties below:

Table 8. Components of LMS-1 [10].

Component	Wt%
Pyroxene	32.8
Glass-rich basalt	32.0
Anorthosite	19.8
Olivine	11.1
Ilmenite	4.3

The table (Table 9) originated from CLASS Exolith Lab below shows the relative abundances of each element detected by X-ray fluorescence (XRF).

Table 9. Oxides [10].

Oxide	Wt%
SiO ₂	46.9
TiO ₂	3.6
Al ₂ O ₃	12.4
FeO	8.6
MnO	0.6
MgO	16.8
CaO	7.0
Na ₂ O	1.7
K ₂ O	0.7
P ₂ O ₅	0.2

LMS-1 contains these chemical elements as minerals described in Table 8 and not necessarily in oxide form as listed in Table 9. The artificial regolith GreenSpar origin is Greenland anorthosite located 85 km southwest of Kangerlussuaq, Greenland and provided by Hudson Resources, Inc., Vancouver, BC, Canada [11]. This anorthosite has 90% plagioclase feldspar and evolved in a low quartz environment, resulting in less than 10% being other minerals. Lunar Highlands are dominated by plagioclase feldspar. The GreenSpar product is available in different size ranges, e.g., GreenSpar 250 ($\leq 250 \mu\text{m}$) and GreenSpar 90 ($\leq 90 \mu\text{m}$) [11]. NASA Johnson Space Center's Astromaterials Research & Exploration Science (ARES) division evaluated the use of GreenSpar 250 for potential use as a component of Lunar Highlands and polar regolith simulants. Table 10 lists the oxides in this simulant.

Table 10. Major oxides of GreenSpar [11].

Major Oxides	Average Wt%
SiO ₂	50.18
Al ₂ O ₃	30.88
Fe ₂ O ₃	0.49
MgO	0.19
CaO	14.58
Na ₂ O	2.63
K ₂ O	0.23
TiO ₂	0.05

Table 10. *Cont.*

Major Oxides	Average Wt%
P ₂ O ₅	0.01
MnO	<0.01
Cr ₂ O ₃	<0.01
V ₂ O ₅	<0.01

Anorthosite is a significant constituent of the lunar crust and plays a crucial role, potentially even a predominant one, in the composition of the lunar regolith. Battler et al. [12] performed research to prepare a simulant with grain size distribution similar to Apollo 16 sample 64,500. Earth-based anorthosite was selected as raw material, and several crushing experiments made. A basic simulant originated from granoblastic facies of the Archean Shawmere Complex of the Kapuskasing Structural Zone of Ontario, Canada. This base simulant had minimal retrogression and was found to be homogeneous and characteristic of Lunar Highlands. Extensive quarry operations were performed due to previous industrial interest in this anorthosite. The availability of this simulant in large amounts is an advantage due to the simple access and extraction of its raw material.

Another simulant based on Shawmere, OB-1 has additional olivine content. This simulant is manufactured by Deltion Innovations, Capreol, ON, Canada, to replicate the Lunar Highlands regolith. It has been crushed to achieve the particle size distribution with glass components of the Apollo 16 sample mentioned above. These simulants are available on a large scale to test drilling and excavation operations and evaluate construction options for future Moon projects. Tables 11 and 12 summarize the key properties of OB1:

Table 11. Physical properties of OB-1 simulant [12].

Property	Value
Mean particle size	82.25 µm
Median particle size	35.97 µm
Specific gravity	3.071
Bulk density	1.815 g/cm ³

Table 12. Major element chemistry of OB-1 simulant [12].

Oxide	Apollo 16 Average Soil wt%	OB-1	Shawmere Anorthosite Average wt%
SiO ₂	45	-	48.28
Al ₂ O ₃	26.7	-	32.01
FeO	-	-	1.34
Fe ₂ O ₃	-	-	0.09
MgO	6.14	-	0.22
CaO	15.3	-	15.43
Na ₂ O	0.457	-	2.38
K ₂ O	0.12	-	0.16
TiO ₂	0.595	-	0.05
P ₂ O ₅	-	-	0.01
MnO	-	-	0.01
Cr ₂ O ₃	-	-	-
V ₂ O ₅	-	-	-

2.2. Frequently Applied Materials for Space Application Subjected to Possible Abrasive Conditions

2.2.1. Requirement for Target Materials

Scopus, Web of Knowledge, and Google Scholar have a wealth of published articles on the conditions and characterization of space. A common feature is that, in addition to vacuum and other pressure conditions, radiation and temperature conditions, as well

as local weather conditions, play a prominent role. A number of papers describe the characterization and expected effects of dust storms in Martian conditions.

Based on three authoritative review summaries [13–15] and some specific articles [16–22], the impacts on structural materials and their characteristics can be summarized as follows. As it is concluded in [14], outer space encompasses various unique environments and forces that differ significantly from those experienced on Earth. These include high-energy charged particles, ultraviolet (UV) radiation, meteoroids, and orbital debris [16]. These factors can have detrimental effects on the behavior of construction materials and can alter fundamental aspects of loading and mechanics. Essentially, there are three key distinctions between the environments of Earth, Moon, and Mars. These differences pose critical challenges and are commonly classified as (1) absence of atmosphere, (2) extreme radiation, and (3) variations in gravity. Earth’s atmosphere consists of a specific gas composition, primarily oxygen (21%) and nitrogen (78%), with traces of carbon dioxide, neon, and others. The Moon is considerably smaller with correspondingly lower gravity and technically lacks an atmosphere. Mars possesses an atmosphere about 100 times thinner than Earth and mainly consists of carbon dioxide, nitrogen, and argon [17]. The Moon and Mars share the characteristic of having a very thin atmosphere, which offers limited protection against meteorites and micrometeorites. Lindsey [18] highlighted that micrometeorites can reach velocities of 20–70 km/s. Toutanji et al. [19] examined the impact of similar particles, firing projectiles weighing 1.4×10^{-4} g into concrete specimens at a speed of 5.9 km/s. The result was the formation of craters with diameters of 13 mm. These experiments, along with the investigations conducted by Nealy et al. [20], underscore the destructive nature of meteorite impacts, the necessity for effective protection against larger meteorites, and the importance of durable and resilient construction materials. Due to the absence of an atmosphere, temperature fluctuations and low pressure are prevalent. On the Moon, the temperature shifts between -173 and 127 °C, while it remains intensely cold on Mars at about -57 °C. The adverse effects of a vacuum are magnified with the absence of an atmosphere. In comparison, the vacuum of space varies from 3×10^{-13} kPa on the Moon to 0.7 kPa on Mars (in contrast to 101.3 kPa on Earth). Under vacuum conditions, materials can experience outgassing, releasing volatile substances. Kanamori et al. [21] investigated the long-term exposure of mortar to a vacuum. Although certain mortar specimens exposed to a vacuum exhibited higher strength compared with those cured with water, the research concluded that vacuum conditions accelerated water loss. Concerning the development of some rover-type and robotic applications, Table 13 gives some features about the Moon and Mars and nearby Earth analog exoplanets.

Table 13. Key differences between Earth, Moon, Mars, and other exoplanets [14].

Parameter	Earth	Moon	Mars	Kepler-	Proxima Centauri b
Total mass compared with Earth (%)	-	1.2	10.7	190	80–110
Approximate distance from Earth (km)	-	3.84×10^5	2.25×10^8	1.32×10^{16}	3.9×10^{13}
Day period (h)	23.9	655.7	24.7	-	-
Revolution period (days)	365.3	27.3	686.9	384.8	11.2
Average surface temperature (°C)	13	-30	-57	-8	-39
Atmospheric pressure (kPa)	101.3	Negligible	0.7	Unknown	Unknown

2.2.2. Materials for Drive System Units: Gears, Shafts, Cams, Guideways, Bushings Steels [15]

Steels are often used only where lighter materials cannot be specified due to the unsuitability of their mechanical, tribological, or chemical properties. Only high-strength steels (ultimate tensile strength (UTS) > 1000 MPa) are usually specified for use in space-craft mechanisms. Maraging (martensitic) steels offer a combination of very high strength, good ductility, and fracture toughness and are used in applications where weight saving is of paramount importance. Precipitation hardening steels offer a combination of good

corrosion resistance and high strength. In the as-quenched condition, these materials can be relatively easily machined because martensite is relatively soft. Quenched and tempered steels depend on their high strength, hardness, and wear resistance in the formation of a metallographic phase called martensite. Martensite is brittle and must be tempered to improve its ductility and toughness for most engineering applications. The two most commonly specified quenched and tempered steels for tribological applications in spacecraft are AISI 440C (ASTM A276) and AISI 52100 (ASTM A295). These materials are almost always used for rolling elements such as bearings.

The maximum continuous operating temperature of AISI 440C is 240 °C; however, special heat treatments and compositions allow use in the range of −269 to −315 °C.

AISI 52100 will operate at up to 150 °C without distortion; however, the maximum continuous operating temperature is 125 °C.

AISI 52100 is used for rolling element bearings because of its high hardness and excellent wear and fatigue resistance.

17/4PH—precipitation hardening steel is widely used across a broad spectrum of industries. It combines high strength and good corrosion properties. It can be hardened between 482 and 621 °C and air-cooled, thereby eliminating scaling and minimizing distortion. It maintains good ductility at sub-zero temperatures. It is magnetic.

17/5PH—similar properties to 17/4. It is ferrite-free and, therefore, has improved notch toughness and better forgeability. 15/5PH was developed as a refinement of 17/4PH.

17/7PH—similar properties to 17/4. Good mechanical properties to 480 °C and superior corrosion resistance. Used for aircraft structural parts, flat and round springs, and drawn, bent, or formed parts.

Alloys, such as Inconel 718, are used occasionally for spacecraft tribo-components instead of steels, where there is a need for a higher temperature capability.

Inconel 600 is usually used for severely corrosive environments at elevated temperatures. This alloy exhibits outstanding resistance to stress corrosion cracking. It should be noted that Inconel 600 cannot be hardened through heat treatment methods.

Inconel 718 is an age-hardened high-strength alloy suitable for service in the temperature range −253 to 700 °C. It has good fatigue and stress rupture properties and good corrosion resistance.

Inconel X-750 is a nonmagnetic alloy that can be age hardened, commonly chosen for its favorable corrosion and oxidation resistance, as well as its high resistance to creep rupture. Initially designed for applications in gas turbines and jet engines, this alloy is also well suited for springs due to its exceptional relaxation resistance. It maintains good strength and ductility even at extremely low temperatures, reaching as low as −253 °C. Moreover, Inconel X-750 exhibits commendable resistance to stress corrosion cracking.

PE16 is a wrought nickel alloy specifically designed to withstand high-temperature conditions. It undergoes age hardening and possesses exceptional creep resistance.

Aluminum Alloys [14,15]

The progress of modern aviation and exploration of outer space has gone through the engineering of aluminum alloys. As directly taken from a NASA technical report [23], “Chosen for its lightweight and able to withstand the stresses that occur during ground and launch operations, aluminum has been used on Apollo spacecraft, the Skylab, the Space Shuttles, and the International Space Station.”

Aluminum alloys are selected for use in spacecraft and other mechanisms because of their low density and high specific strength. The disadvantages of aluminum alloys are their low stiffness, low hardness, high thermal expansion coefficient, and susceptibility to high adhesive wear and galling. In self-mating sliding contacts in a vacuum, aluminum alloys exhibit high and variable friction coefficients ($\mu > 0.5$). Aluminum alloys are widely used in spacecraft mechanisms but must receive surface treatments to improve their tribological properties. Most of the alloys contain varying amounts of Mg, Cu, Si, and Zn as strengthening additions. They are summarized in Table 14.

Table 14. The most typical aluminum alloys [11].

Alloy Group	Wrought Alloys Major Alloying Elements	Alloy Group	Cast Alloys Major Alloying Elements
1XXX	99.00% minimum aluminum	1XX.0	99.00 percent minimum aluminum
2XXX	Copper	2XX.0	Copper
3XXX	Manganese	3XX.0	Silicon with added copper and/or magnesium
4XXX	Silicon	4XX.0	Silicon
5XXX	Magnesium	5XX.0	Magnesium
6XXX	Magnesium and silicon	6XX.0	Unused series
7XXX	Zinc	7XX.0	Zinc
8XXX	Other elements	8XX.0	Tin
9XXX	Unused series	9XX.0	Other elements

1000 series: commercially pure aluminum. These have low strength but are very ductile.

2000 series: alloy additions of copper and magnesium. High strength. These are heat treatable. Copper additions reduce corrosion resistance.

5000 series: magnesium is the main alloying element. Non-heat treatable. Their mechanical properties are better than 1000, 3000, and 4000 series. Good corrosion resistance.

6000 series: Heat treatable. Corrosion resistance is inferior to the 5000 series but sufficient for general engineering purposes.

7000 series: specialized alloys used mainly in aerospace applications. Heat treatable. The presence of copper reduces corrosion resistance and weldability, and strength properties are superior.

The main groups used in the aerospace industry are the 2XXX, 6XXX, and 7XXX (wrought) and Al-Si casting alloys. These materials reach high strengths after specific conditioning. Such series are age hardenable, and they can be strengthened by this process under heat treatment [24]. The mechanical properties may decrease with an increase in temperature above 100 °C. However, in general, the strength, ductility, and toughness of aluminum may increase in low temperatures.

Titanium Alloys [14,15]

Titanium alloys are widely used in spacecraft mechanisms because of their relatively low density, excellent mechanical properties, and high resistance to stress corrosion cracking. The main disadvantage of titanium alloys is their poor adhesive wear resistance, and surface treatments are vital to improve the tribological performance. In self-mating sliding contacts in a vacuum, titanium alloys will exhibit high and variable friction coefficients ($\mu > 0.5$). Titanium alloys, of which IMI 318 and IMI 550 are listed, are in ESA PSS-01-701 (ESA preferred materials). Thermomechanical and heat treatment procedures have been devised to ensure that the alloys IMI 318 and IMI 550 provide the optimum balance of mechanical properties for a wide range of applications.

Copper-Based Alloys [14,15]

There has been limited use of bronzes in spacecraft mechanisms. They are used principally as leaded bronze cages in ball bearings lubricated with ion-plated lead coatings.

Phosphor bronzes contain residual phosphorus (≥ 1 wt%), which imparts high hardness. Phosphor bronzes have high wear resistance and hardness and moderately high strength. UNS C9 0700 is so widely used for gears that it is often termed gear bronze.

Aluminum bronzes have good corrosion resistance and higher fatigue limits than any other cast copper alloy and can be used at temperatures up to 400 °C without significant loss of strength. They also tend to be more resistant to galling than manganese bronzes. These materials are suitable for heavy-duty service (valve guides, bearings, screw-down nuts, and slippers) and precision machinery.

Manganese bronzes have better toughness than aluminum bronzes of equivalent tensile strength and do not require heat treatment, as strength is developed by solid

solution hardening. Lead may be added to lower-strength grades to improve machinability but should not exceed 0.1 wt% in higher-strength alloys. Manganese bronzes are specified for applications that require high strength, hardness, and resistance to mechanical shocks, such as large gears, bridge turntables, gun tracks, and ordnance recoil parts. Their upper temperature limit for use is around 230 °C.

High leaded, tin bronzes are used where a softer metal than phosphor bronze is required for low load and low sliding speed applications. UNS 93700 (80-10-10) is an excellent general bearing alloy, especially well suited for applications where lubrication may be deficient, such as bearing cages, for use in a vacuum. LB9 is used extensively for cages in bearings lubricated with ion-plated lead.

Beryllium–copper alloys possess a unique combination of mechanical and physical properties, which makes them ideal for selected applications in spacecraft mechanisms. These properties include high strength and hardness, high fatigue and creep resistance, and good electrical and magnetic characteristics. In self-mating sliding contacts in a vacuum, Be–Cu alloys will exhibit high and variable friction coefficients ($\mu > 0.5$). Be–Cu alloys are used for springs that apply load to sliding contacts and for reed switches (gold coated). Cu-1.8 wt% Be, 0.3 wt% Co–Ni (CDA 170) is listed in ESA PSS-01-701.

High-Density Alloys [15]

Tungsten-based alloys containing small amounts of nickel–copper binders have high densities (comparable to tungsten) and offer improved machinability compared with pure tungsten. They are used in engineering applications requiring high inertial forces, e.g., counterweights, gyroscope rotors, and balancing weights. They have been tested as candidate materials for impacting surfaces in space.

Polymer Composites [13,15]

The tribological and mechanical properties of a polymer can be modified by incorporating solid fillers into the matrix. Fibers (10–20 wt%) are added to engineering polymers to increase their stiffness, strength, and creep resistance. These fibers are typically 5–10 μm in diameter and can be continuous, milled, or chopped. Fiber size and orientation have a great effect on wear resistance and on mechanical properties. Polyamide (Kevlar), glass, carbon, nylon, polyester, and cotton are all commonly specified as fiber reinforcements. Asbestos was used in the past, but is now largely avoided on safety grounds. Glass fibers are harder than many metals and may cause abrasive wear. Kevlar, carbon, and graphite fibers are used to enhance strength, stiffness, and creep resistance. Like graphite lubricants, graphitic fibers have poor tribological properties in a vacuum.

Carbon or glass-fiber-filled acetal and fiber-reinforced and filled PTFE (Rulon) are commonly specified for low-precision gears in spacecraft mechanisms. Duroid is a PTFE/glass and MoS₂ composite that was commonly used as a cage material for ball bearings but is no longer manufactured. PGM-HT is a material of similar composition to Duroid. For some applications requiring extreme strength (e.g., high speed bearing cages), woven three-dimensional cloth (glass, cotton, or carbon fiber) preforms can be impregnated with phenolic or polyester resins. These materials are supplied under the trade names Orkot, Tufnol, Ferrobestos, Railko, and Tenmat. Promising material is concerning temperature resistance, strength and wear resistance, high energy radiation resistance, and the different grades (natural and reinforced) of PEEK.

Ceramics [14,15]

Light engineering ceramics, such as silicon nitride, silicon carbide, and alumina, all have high intrinsic strength and hardness. Silicon nitride has high flexural strength (greater than 1000 MPa at temperatures up to 1100 °C), high stiffness, high wear resistance, hardness, good oxidation and corrosion resistance, and good thermal shock resistance because of the strength of the Si–N bonds and a low thermal expansion coefficient. Silicon nitride components are usually prepared by hot pressing, although the process is expensive. Only

simple shapes can be produced, and the surface finish of components is inferior to the best finishes attainable with steel. High-precision, hot pressed Si₃N₄ (for bearings) is commercially available. Silicon nitride rings are also available but have not hitherto been favored because of concerns over thermal expansion mismatch and cracking under tensile stresses (particularly at launch). Tungsten carbide balls are also available, their properties being similar to silicon nitrides but having a higher density.

2.2.3. Summary of Possible Tribomaterials for Space Applications

The following table (Table 15) gives a summary of tribological information on moving element materials based on the literature [13–15].

Table 15. Summary of tribological information of material of moving elements.

Material Families	For Tribological Applications			
	Not Recommended or Strongly Limited	May Be Proposed with Surface and Structural Modifications	May Be Suggested (Some Typical Application)	Possibly in Abrasive Condition
Maraging steel		+	+	+
Precipitation hardening steel		+	?	+
Quenched and tempered steels		+	+	+
Steel alloys: Cr, Ni alloyed steel, austenitic steels, multiphase steels				?
Aluminum alloys	+	+	?	?
Titanium alloys		+	?	?
Phosphor bronzes			+	?
Aluminum bronzes			+	?
Manganese bronzes			+	?
High-leaded tin bronzes			+	?
Beryllium–copper alloys	+			-
Tungsten-based alloy		+	?	?
Polymer composites			+	+
Ceramics			+	?

Abrasive tested space materials published in articles [25–58] are analyzed and summarized in Table 16. One article may deal with two or more materials under different conditions that are taken into account in the table.

Table 16. Number of cases about materials with its conditions.

	Room Conditions	Vacuum or Neutral Gas and Room Temperature	Low and High Temperatures	Vacuum and High/Low Temperatures	With Simulants
Structural steel	7	2	11	1	1
Martensitic steel	6				
Manganese steel and other alloyed steel	8		1		
Stainless steel	3	2	4		
Ceramics	11	1	1		
Rubber/elastomer	12				
Polymer/composite	3	4	1		1
Alloyed cast irons	3				
Titanium alloy	1				
WC-based sintered or hard metal	3		1		
Aluminum/coated and alloys	1	3	1	1	2

2.2.4. Identified Rotary Shaft and Seal Materials

Identified rotary shaft and seal materials (ESMATS Past Papers Database) already tested, applied, and published [24,52,59–68] are concluded in Table 17.

Table 17. Shaft and seal (machine element) materials for space tested and reported.

Shaft/Machine Elements	Room Conditions	Vacuum or Neutral Gas and Room Temperature	Low and High Temperatures	Vacuum and High/Low Temperatures	With Simulants
Aluminum	Al2024 Anodized aluminum	Anodized aluminum	Al2024, Al7000 series		Anodized aluminum
Copper			Beryllium copper Nitronic 60		
Steel	Stainless steel	Stainless steel	(stainless steel) 400C, S2100 Ti6Al4V		Stainless steel
Titanium Seal					
Polymer	PCTFE, PI/MoS ₂ PTFE 3x	PTFE 3x	PCTFE, PI/MoS ₂		PTFE 3x
Hybrid structure			Polymer/metal		

2.2.5. Literature Analyses of Rotary/Reciprocating Shaft–Seal Mechanisms Possibly Subjected to Abrasive Conditions

Articles on different space mechanisms [23,52,60,68–94] are evaluated. Mechanisms, shaft materials, sealings, and bearing solutions are identified. In Tables 18 and 19, the conclusions are summarized.

Table 18. Grouping of mechanisms.

Mechanism	Number of Case
Any rover applications	4
Open–close mechanisms	6
Positioning mechanisms/mechatronics	4
Berthing—docking	4
Robotic arm	4
Doors	4
Other rotary/reciprocating shafts	5

Table 19. Shaft and seal materials identified in mechanisms.

Shaft Materials	Number of Cases
Cooper–beryllium alloy	4
Titanium alloy	7
Al and Al alloy	9
Stainless steel	9
Other steel alloys	4
Seal materials	Number of cases
PTFE	19
PTFE—composite	4
Hybrid: metal/polymer combinations	1
Metallic	3
Other polymers (HPM, UHMW-PE. . .)	6

As it is reported, stainless steel and Al versions are commonly applied materials as shaft materials, while seal solutions are preferred of PTFE natural or other grades even

with metallic combinations. The reported cases mainly belong to the low-speed sliding mechanism, where the sliding speed can vary between 0–0.1 and 0–0.2 m/s, with both roller (ball) and slide bearing solutions.

3. Review on Application of Martian and Lunar Simulants

Several application examples are to be considered for the selection of simulants. For instance, on Mars, layers of dust accumulate on solar panels due to atmospheric transport, diminishing their efficiency. Additionally, dust storms disperse particles across exposed surfaces. On the Moon, the lack of atmosphere prevents the transportation of particles by winds. However, various activities, such as firing descent thrusters, rover wheel movements, solar charging, and instrument interactions with lunar regolith, can stir up dust and contaminate surfaces. T. Tattusch et al. [95] observed a variety of effects contingent upon the celestial body on which a space system operates. For the ESA DEAR (Dusty Environment and Robotics) project, a special test bench was set up to perform environmental tests. Four different simulants, ISO reference dust eskal 60, ISO reference dust eskal 150, Lunar Regolith Simulant TUBS-T, and Lunar Regolith Simulant TUBS-M, have been applied. The advantages of ISO simulants were nonhygroscopic behavior and simple handling and storage, while the drawback was different particle size distributions from the real samples. TUBS lunar regolith simulants were very similar to real lunar samples in chemistry, particle size distribution, and particle shape. However, sharp-edged fine dust required special safety instructions and precautions.

Budzyn et al. [96] performed topology optimization as a design method to enhance hardware performance in the lunar dust environment. The knowledge gained from the Apollo missions revealed that lunar regolith particles possess sharp edges, carry electrostatic charges, exhibit adhesive properties, and pose a significant risk to mission hardware. They can infiltrate gaps between mechanical elements and cause damage, particularly in scenarios involving rigid body relative displacements. In this context, an alternative design strategy for lunar surface hardware is proposed. The authors suggest utilizing compliant mechanisms to create monolithic structures that inherently withstand lunar dust effects. To facilitate the design of compliant mechanisms, topology-optimization-based design methods are to be adopted. Topology optimization aims to optimize material distribution for a given design space and boundary conditions to maximize the performance of the design. The study explores several MATLAB routines that can assist in topology optimization for compliant mechanisms. Each routine's advantages and disadvantages are outlined, and their application to a compliant force inverter is demonstrated.

During the preliminary assessment of seals for dust mitigation in mechanical components for Martian and lunar surface systems, various factors were taken into account by E.T. Baumgartner [97] and Harrington et al. [98]. Delgado et al. [52] carried out component-level experiments to evaluate the effectiveness of spring-loaded Teflon seals in preventing a lunar simulant from entering the gearbox, motor, and bearing housings of mechanical components. The PTFE seals of three different diameters were tested: 9.5, 19, and 38 mm. Tests were conducted at 20 RPM up to 10,000 cycles (number of rotations) in dry-room and vacuum conditions using the lunar simulants JSC-1A and LHT-2M. Baseline tests were performed in a dry room without a simulant. In their tests, no simulant was observed to pass through the seal–shaft interface, and a minimal amount of wear was observed on both the seal and shaft. The seal weight loss was minimal with only PTFE 'flakes' observed on the downstream side of the seal, and the shaft profilometry generally showed a slight deterioration in shaft surface roughness with simulant use. The inconsistencies between surface roughness and seal weight loss require further analysis. To further evaluate endurance, future tests are planned using NASA Lunar Surface System architecture shaft sizes and relevant operating conditions.

4. Discussion and Conclusions

Huge amounts of simulants are available to model different space objects, such as asteroids, planets, and comets [99]. Selection criteria for lunar and Martian simulants shall be defined based on the availability, chemical/physical properties, and application use cases. A decision has been made also about technical criteria for our tribological testing.

Additional, nontechnical selection criteria have been considered. The preparation of certain simulants requires a costly and long process and results in a small amount of simulants. Selection criteria were introduced to reflect the delivery lead time and cost of simulant/kg. Considering our technical review results, the mineralogical form and particle shape of the simulant are more important than the pure chemical substance ratio. Simulants are selected that represent more the landing site and are as similar as reasonably possible to the real soil samples. It is preferred to have high mineralogical fidelity, but considers limitations due to Earth-based component sourcing.

According to these two criteria, and considering the contradiction of using Earth-based raw material to prepare Moon and Mars simulants, the core selection requirements are

- Level of mineralogical fidelity: particle shape and form relevant to abrasion test allowing for good representativity of the test with real lunar/Martian regolith;
- Particle size distribution;
- Density and gravity;
- Information basis of the preparation of simulants.

The following tables (Tables 20 and 21) are mapping the simulants and the criteria described above.

Considering the options listed in Tables 20 and 21, four different simulants have been identified for our purpose.

LMS-1: The first sample aims to represent a generic or average mare location on the Moon. It is a highly accurate mineral-based simulant specifically tailored for this purpose. Instead of being composed of a single terrestrial lithology, it successfully replicates the lunar regolith's texture by combining mineral and rock fragments (polyminerale grains) in precise proportions. The simulant's particle size distribution is designed to match that of typical Apollo soils.

LHS-1: The second sample is designed to simulate Lunar Highlands. It is a mineral-based simulant suitable for a generic or average highlands location on the Moon. Like the previous simulant, it does not consist of a single terrestrial lithology. However, it accurately captures the texture of lunar regolith. The particle size distribution of this simulant is carefully adjusted to resemble that of typical Apollo soils.

MGS-1: The third sample aims to represent Mars. It serves as a mineralogical standard for basaltic soils found on Mars, developed based on quantitative mineralogy obtained from the MSL Curiosity rover. Specifically, it seeks to replicate the composition of the Rocknest windblown soil, which chemically resembles other basaltic soils at various landing sites, making it a suitable "global" basaltic soil representation. The development process involves sourcing individual minerals, including appropriate treatment of the X-ray amorphous component.

JEZ-1: The fourth sample is designed to mimic the anticipated materials found in the Jezero crater deltas, which are being investigated by the NASA Mars 2020 rover. This simulant is a blend of the previous sample (Sample 3—MGS-1) with smectite clay, Mg-carbonate, and additional olivine. The selection of these components is based on their detection through orbital remote sensing in the Jezero delta deposits.

Table 20. Comparison of lunar simulants based on mineralogical fidelity, price, and availability.

Simulant Type	Name	Supplier	Country	Description	Particle Size Range	Mineralogical Fidelity	Price	Availability
Lunar Mare	LMS-1	Exolith Lab	USA	High mineralogical fidelity	<0.04 µm–300 µm		USD 35/kg	Available
	OPRL2N	Off Planet Research	USA	Mechanical simulant	Apollo 17 PSD		About USD 80/kg	Available
	UoM-B and UoM-W	University of Manchester	UK	Low-fidelity, angular grain shapes	B: 0.1–0.7 mm W: <125 µm			From feedstock supplier
	TUBS-M	TU Braunschweig	Germany	ISRU-oriented base simulant, customizable	0–2 mm			
Lunar Highland	LHS-1	Exolith Lab	USA	High mineralogical fidelity, Subangular grains, lower specific gravity	<0.04 µm–400 µm		USD 35/kg	Available
	GreenSpar	Hudson Resources	Greenland	High anorthite content	<250 µm or <90 µm	High An%	Unknown	Available
	OPRH2N	Off Planet Research	USA	Mechanical simulant	Apollo highland sample PSD average	High An%	About USD 80/kg	Available
	OB-1	Deltion Innovations	Canada	High glass content, angular grains, high specific gravity	Apollo 16 sample 64,500 PSD	High An%	Unknown	Unknown
	TUBS-T	TU Braunschweig	Germany	ISRU-oriented base simulant, customizable	0–2 mm	Customizable		

Color coding means the following: mineralogical fidelity (compared with their respective reference material): red: low; yellow: moderate fidelity; green: high. Price of 5 kg simulant (product only): red: over EUR 500; yellow: unknown; green: less than EUR 500. Availability (5 kg or more): red: not available; yellow: unknown; green: available for acquisition.

Table 21. Comparison of Martian simulants based on mineralogical fidelity, price, and availability.

Simulant Type	Name	Supplier	Country	Description	Particle Size Range	Mineralogical Fidelity	Price	Availability
Mars	MGS-1	Exolith Lab	USA	High mineral, chemical, volatile, and spectral fidelities.	>0.04 μm –600 μm		USD 35/kg	Available
	ES-x	Varies	Europe	Geotechnical simulants in different size ranges.	1: <10–32 μm 2: ~ >30–125 μm 3: ~>30–20,000 μm 4: ~0.1–500 μm			Some available from ESA or supplier
	OUCM OUEB OUHR OUSR	Open University	UK	Astrobiology simulants. Each has a standard composition (–1) and adjusted Fe^{2+} concentration (–2).	200–2000 μm			
	JSC Mars-1	NASA JSC	USA	Spectral analogue, supports general scientific and engineering studies.	<1 mm		Only pay for shipping	Available
	P/S-MRS	DLR	Germany	For Raman spectral studies.	<1 mm		Unknown	Unknown
Mars Jezero	JEZ-1	Exolith Lab	USA	MGS-1 mixed with smectite, Mg-carbonate, and additional olivine.	<0.04–500 μm		USD 35/kg	Available

Color coding means the following: mineralogical fidelity (compared with their respective reference material): red: low; yellow: moderate fidelity; green: high. Price of 5 kg simulant (product only): red: over EUR 500; yellow: unknown; green: less than EUR 500. Availability (5 kg or more): red: not available; yellow: unknown; green: available for acquisition.

Figure 2 shows the selected soil simulants.

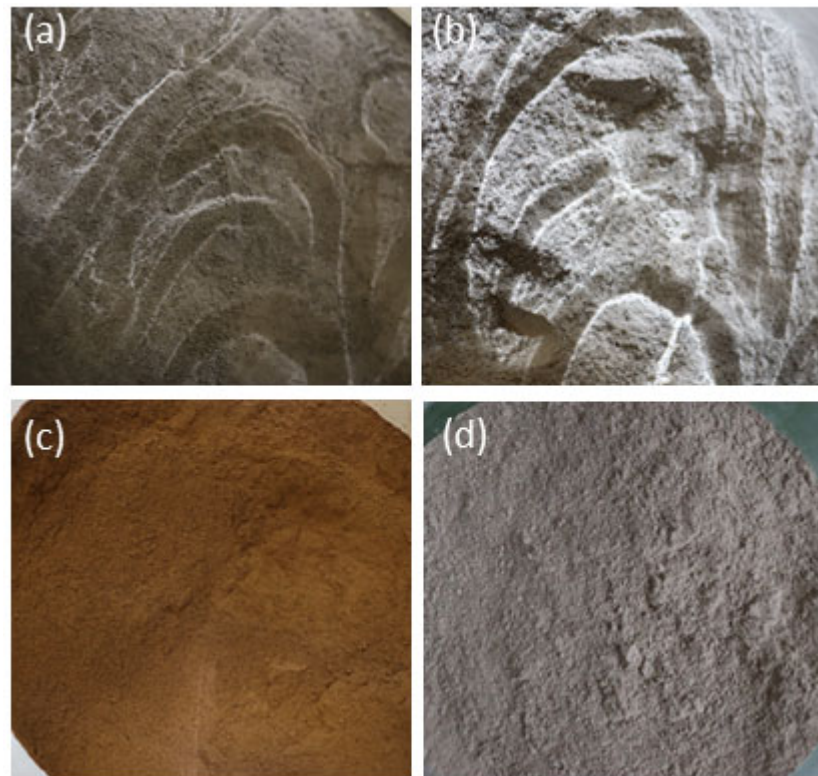


Figure 2. Selected soil simulants: (a) LMS-1 Lunar Mare, (b) LHS-1 Lunar Highlands, (c) MGS-1 Mars General, (d) JEZ-1 Mars Jezero.

Concerning the structural materials of shaft solutions paired with any kind of sealings against abrasive particles, the following order can be seen based on numerous published case studies and research reports (the most frequent published materials at the beginning of the list, the less frequent ones at the end):

- Structural and martensitic and manganese steel grades;
- Stainless steel grades;
- High-strength aluminum, anodized;
- Other aluminum alloys;
- Polymer/composites;
- Ceramics;
- Ti alloys.

The following structural materials were selected for the further detailed study of the abrasion effect and the research of a sealed rotating shaft subjected to simulant particles:

- Rotary shaft materials: stainless steel AISI 440C and hard anodized Al 7075 (Figure 3);
- Sealing materials: natural PTFE and composite PTFE/15%GF+5%MoS₂ lipseals and packings (Figure 4).

The scope of the current paper is focusing on the selection of shaft/sealing and lunar/Martian simulants for the tests; review and discussion of the test results are subject to a separate scientific communication.

Diversification of the country of origin is observed in the field of preparation of lunar and Martian simulants. In 2020, the majority of the simulant source was linked to NASA (US) and ESA (Europe). In 2023, out of the 91 simulants listed in [99], fewer than half of the samples were prepared in the USA (43 simulants) and only 20 in the EU. The future trend is expected to grow the simulant manufacturing capability in the APAC region (especially in China and Japan) and in the EU. It has been proved to be a commercial opportunity also

for academic and university spin-off companies to generate artificial soil samples more for the region of interest of the local scientific community.

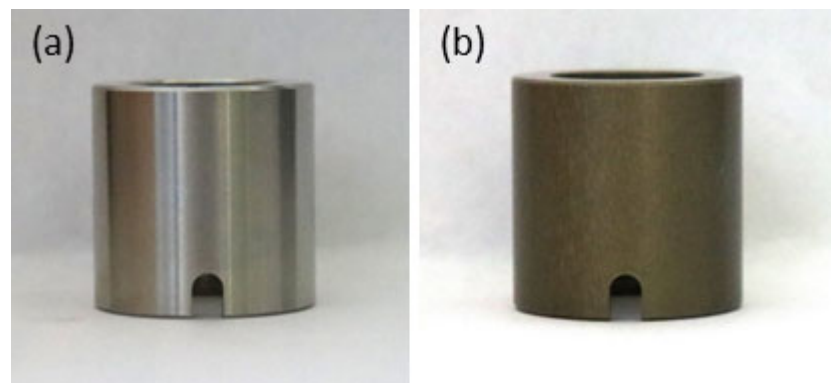


Figure 3. (a) Stainless steel and (b) anodized Al shaft samples for further research.

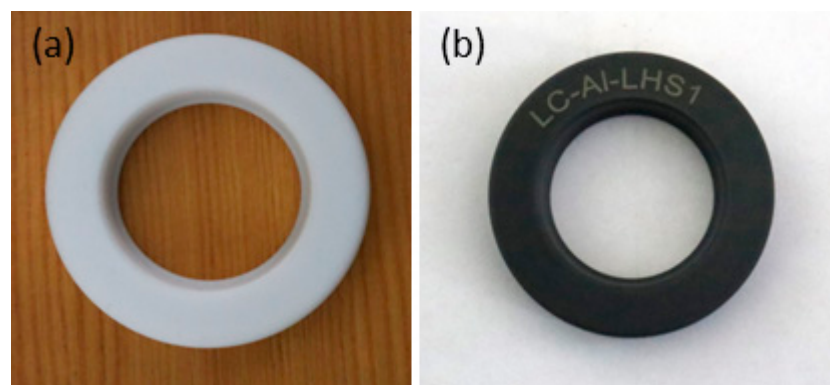


Figure 4. (a) Natural and (b) composite PTFE lipseal samples.

Interest in lighter but more abrasive-resistant moving mechanical parts is shifting the research focus from stainless steel to aerospace-grade alloys and nonmetallic structures. Not only the mechanical properties but the applicable heat range is extended to the magnitude where space application can be a relevant option. Three-dimensionally-printed parts are in the main area of interest for this purpose [100].

There is also continuous development and improvement in the field of structural materials exposed to aggressive abrasion effects. The delicate balance that material developers must keep in mind is launch-load compliance (excellent specific strength), low density, and compliance with space conditions and impacts. Applications and developments so far have proven that there are few materials that can “purely” meet these complex requirements. The developments are shifting towards alloys, surface coatings, modified surfaces, composites, and hybrid composites, despite the fact that they are also trying to put production processes on a new foundation (3D printing, space metallurgy using external materials, implementation of technology transfer). One thing is certain: the priority of safety aspects cannot ignore the most thorough terrestrial modelling and knowledge of the exact response of mechanical systems to space requirements.

Author Contributions: Conceptualization: G.B. and G.K.; writing—original draft preparation: Á.K., H.S., G.B. and G.K.; writing—review and editing: Á.K., G.K. and G.B.; visualization: R.K. and L.Z.; supervision and project administration: G.B. and G.K. All authors have read and agreed to the published version of the manuscript.

Funding: This research was funded by European Space Agency (ESA), Contract No. 4000136800/21/NL/CBi.

Data Availability Statement: Data is available upon request from first/corresponding authors.

Acknowledgments: The authors express special thanks to Kamini Manick, SACF Curator and Laboratory Coordinator, and Xiaochen Zhang, SACF Young Graduate Trainee, for their contribution to the data collection and support of the analysis. The authors would like to acknowledge the support of Ewelina Ryszawa. Special thanks to Stefan Linke and Joel James Patzwald, Technische Universität Berlin, for the TUBS-T and TUBS-M simulant samples.

Conflicts of Interest: The authors declare no conflict of interest.

References

1. Gouache, T.P.; Patel, N.; Brunskill, C.; Scott, G.P.; Saaj, C.M.; Matthews, M.; Cui, L. Soil simulant sourcing for the ExoMars rover testbed. *Planet. Space Sci.* **2011**, *59*, 779–787. [CrossRef]
2. Alexander, M. Mars Transportation Environment Definition Document. NASA Technical Memorandum, no. 210935. 2001. Available online: <http://www.sti.nasa.gov> (accessed on 7 June 2023).
3. Newson, T.; Ahmed, A.; Joshi, D.; Zhang, X.; Osinski, G.R. Assessment of the Geomechanical Properties of Lunar Simulant Soils. in *Earth and Space 2021: Space Exploration, Utilization, Engineering, and Construction in Extreme Environments*. In Proceedings of the 17th Biennial International Conference on Engineering, Science, Construction, and Operations in Challenging Environments, Online, 19–23 April 2021; pp. 146–156. [CrossRef]
4. Böttger, U.; De Vera, J.P.; Fritz, J.; Weber, I.; Hübers, H.W.; Schulze-Makuch, D. Optimizing the detection of carotene in cyanobacteria in a martian regolith analogue with a Raman spectrometer for the ExoMars mission. *Planet. Space Sci.* **2012**, *60*, 356–362. [CrossRef]
5. Allen, C.C.; Morris, R.V.; Karen, M.J.; Golden, D.C.; Lindstrom, M.M.; Lockwood, J.P. Martian Regolith Simulant JSC Mars-1. In *Lunar and Planetary Science Conference XXIX, 1998*, no. Table 2. p. 1690. Available online: <https://ui.adsabs.harvard.edu/abs/1998LPI...29.1690A/abstract> (accessed on 7 June 2023).
6. Cannon, K.M.; Britt, D.T.; Smith, T.M.; Fritsche, R.F.; Batchelor, D. Mars global simulant MGS-1: A Rocknest-based open standard for basaltic martian regolith simulants. *Icarus* **2019**, *317*, 470–478. [CrossRef]
7. Just, G.H.; Joy, K.H.; Roy, M.J.; Smith, K.L. Geotechnical characterisation of two new low-fidelity lunar regolith analogues (UoM-B and UoM-W) for use in large-scale engineering experiments. *Acta Astronaut.* **2020**, *173*, 414–424. [CrossRef]
8. Linke, S.; Windisch, L.; Kueter, N.; Wanvik, J.E.; Voss, A.; Stoll, E.; Schilde, C.; Kwade, A. TUBS-M and TUBS-T based modular Regolith Simulant System for the support of lunar ISRU activities. *Planet. Space Sci.* **2020**, *180*, 104747. [CrossRef]
9. Simulants, Feedstocks, and Additives. Available online: <https://www.offplanetresearch.com/simulants-feedstocks-and-additives> (accessed on 9 May 2022).
10. Lunar Mare (LMS-1) High-Fidelity Moon Dirt Simulant. Available online: <https://exolithsimulants.com/collections/regolith-simulants/products/lms-1-lunar-mare-simulant> (accessed on 10 May 2022).
11. Gruener, J.E.; Deitrick, S.R.; Tu, V.M.; Clark, J.V.; Ming, D.W. Cambon, Greenland ‘White Mountain’ Anorthosite: A New Lunar Polar Regolith Simulant Component. 2020. Available online: <https://hudsonresourcesinc.com/nasa-greenspar-lunar-simulant-abstract-greenland-white-mountain-anorthosite-a-new-lunar-polar-regolith-simulant-component/> (accessed on 7 June 2023).
12. Battler, M.M.; Spray, J.G. The Shawmere anorthosite and OB-1 as lunar highland regolith simulants. *Planet. Space Sci.* **2009**, *57*, 2128–2131. [CrossRef]
13. Chen, J.; Ding, N.; Li, Z.; Wang, W. Organic polymer materials in the space environment. *Prog. Aerosp. Sci.* **2016**, *83*, 37–56. [CrossRef]
14. Naser, M.Z.; Chehab, A.I. Materials and design concepts for space-resilient structures. *Prog. Aerosp. Sci.* **2018**, *98*, 74–90. [CrossRef]
15. Roberts, E.W.; Eiden, M. *A Space Tribology Handbook*; Warrington: European Space Tribology Laboratory: Cheshire, UK, 2013.
16. Lim, S.; Anand, M. Space Architecture Technology for Settlement and Exploration on Other Planetary Bodies—In-Situ Resource Utilisation (ISRU) Based Structures on the Moon. May 2014. Available online: <https://els2014.arc.nasa.gov> (accessed on 7 June 2023).
17. Mars Atmosphere: Facts about the Composition and Climate. Available online: <https://www.space.com/16903-mars-atmosphere-climate-weather.html> (accessed on 18 March 2022).
18. Lindsey, N.J. Lunar Station Protection: Lunar Regolith Shielding. In Proceedings of the International Lunar Conference, Hawaii Island, HI, USA, 16–22 November 2003.
19. Toutanji, H.A.; Evans, S.; Grugel, R.N. Performance of lunar sulfur concrete in lunar environments. *Constr. Build. Mater.* **2012**, *29*, 444–448. [CrossRef]
20. Nealy, J.; Wilson, J.; Townsend, L. *Solar-Flare Shielding with Regolith at a Lunar-Base Site*; NASA Technical Paper; NASA: Washington, DC, USA, 1989.
21. Kanamori, H.; Matsumoto, S.; Ishikawa, N. Long-term properties of mortar exposed to a vacuum. *ACI Spec. Publ.* **1991**, *125*, 57–69. [CrossRef]
22. Duffie, J.A.; Beckman, W.A. *Solar Engineering of Thermal Processes*, 4th ed.; Solar Energy Laboratory University of Wisconsin: Madison, WI, USA, 2013.

23. Uythoven, E.; Mäusli, P.-A.; Toussaint, C.; Udriot, M.; Kneib, J.-P. Design of a Novel Separation Mechanism for High-Power Model Rockets. ESMATS-2021. Available online: <https://www.esmats.eu/esmatspapers/pastpapers/pdfs/2021/uythoven.pdf> (accessed on 10 October 2022).
24. Kanji, S.; Buratynsky, M. Challenges Associated with Testing Mechanisms for a Martian Environment. In Proceedings of the 18th European Space Mechanisms and Tribology Symposium 2019, Munich, Germany, 18–20 September 2019.
25. Penagos, J.J.; Pereira, J.I.; Machado, P.C.; Albertin, E.; Sinatora, A. Synergetic effect of niobium and molybdenum on abrasion resistance of high chromium cast irons. *Wear* **2017**, *376–377*, 983–992. [[CrossRef](#)]
26. Qiu, J.; Fu, Z.; Liu, B.; Liu, Y.; Yan, J.; Pan, D.; Zhang, W.; Baker, I. Effects of niobium particles on the wear behavior of powder metallurgical γ -TiAl alloy in different environments. *Wear* **2019**, *434–435*, 202964. [[CrossRef](#)]
27. Dalai, R.; Das, S.; Das, K. Effect of thermo-mechanical processing on the low impact abrasion and low stress sliding wear resistance of austenitic high manganese steels. *Wear* **2019**, *420–421*, 176–183. [[CrossRef](#)]
28. Mpagazehe, J.N.; Street, K.W.; Delgado, I.R.; Higgs, C.F. An experimental study of lunar dust erosive wear potential using the JSC-1AF lunar dust simulant. *Wear* **2014**, *316*, 79–91. [[CrossRef](#)]
29. Bühler, C.A. Experimental investigation of lunar dust impact wear. *Wear* **2015**, *342–343*, 244–251. [[CrossRef](#)]
30. Sengupta, A.; Kulleck, J.; Van Norman, J.; Mehta, M. Thermal coating erosion in a simulated Martian landing environment. *Wear* **2011**, *270*, 335–343. [[CrossRef](#)]
31. Pei, Z.; Song, R.; Ba, Q.; Feng, Y. Dimensionality wear analysis: Three-body impact abrasive wear behavior of a martensitic steel in comparison with Mn13Cr2. *Wear* **2018**, *414–415*, 341–351. [[CrossRef](#)]
32. Huang, L.; Deng, X.; Li, C.; Jia, Y.; Wang, Q.; Wang, Z. Effect of TiC particles on three-body abrasive wear behaviour of low alloy abrasion-resistant steel. *Wear* **2019**, *434–435*, 202971. [[CrossRef](#)]
33. Li, Y.; Gao, Y. Three-body abrasive wear behavior of CC/high-Cr WCI composite and its interfacial characteristics. *Wear* **2010**, *268*, 511–518. [[CrossRef](#)]
34. Harsha, A.P. An investigation on low stress abrasive wear characteristics of high performance engineering thermoplastic polymers. *Wear* **2011**, *271*, 942–951. [[CrossRef](#)]
35. Huang, L.; Deng, X.; Jia, Y.; Li, C.; Wang, Z. Effects of using (Ti,Mo)C particles to reduce the three-body abrasive wear of a low alloy steel. *Wear* **2018**, *410–411*, 119–126. [[CrossRef](#)]
36. Hu, C.; Wan, X.; Wu, K.; Xu, D.; Li, G.; Xu, G.; Misra, R. On the impacts of grain refinement and strain-induced deformation on three-body abrasive wear responses of 18Cr–8Ni austenitic stainless steel. *Wear* **2020**, *446–447*, 203181. [[CrossRef](#)]
37. Varga, M. High temperature abrasive wear of metallic materials. *Wear* **2017**, *376–377*, 443–451. [[CrossRef](#)]
38. Penagos, J.J.; Ono, F.; Albertin, E.; Sinatora, A. Structure refinement effect on two and three-body abrasion resistance of high chromium cast irons. *Wear* **2015**, *340–341*, 19–24. [[CrossRef](#)]
39. Antonov, M.; Hussainova, I.; Veinthal, R.; Pirso, J. Effect of temperature and load on three-body abrasion of cermets and steel. *Tribol. Int.* **2012**, *46*, 261–268. [[CrossRef](#)]
40. Shah, M.; Bakshi, S.D. Three-body abrasive wear of carbide-free bainite, martensite and bainite-martensite structure of similar hardness. *Wear* **2018**, *402–403*, 207–215. [[CrossRef](#)]
41. Varga, M.; Rojacz, H.; Winkelmann, H.; Mayer, H.; Badisch, E. Wear reducing effects and temperature dependence of tribolayer formation in harsh environment. *Tribol. Int.* **2013**, *65*, 190–199. [[CrossRef](#)]
42. Bakshi, S.D.; Sinha, D.; Chowdhury, S.G.; Mahashabde, V.V. Surface and sub-surface damage of 0.20 wt% C-martensite during three-body abrasion. *Wear* **2018**, *394–395*, 217–227. [[CrossRef](#)]
43. Mukhopadhyay, P.; Kannaki, P.S.; Srinivas, M.; Roy, M. Microstructural developments during abrasion of M50 bearing steel. *Wear* **2014**, *315*, 31–37. [[CrossRef](#)]
44. Nahvi, S.M.; Shipway, P.H.; McCartney, D.G. Particle motion and modes of wear in the dry sand–rubber wheel abrasion test. *Wear* **2009**, *267*, 2083–2091. [[CrossRef](#)]
45. Jokari-Sheshdeh, M.; Ali, Y.; Gallo, S.C.; Lin, W.; Gates, J.D. Comparing the abrasion performance of NiHard-4 and high-Cr-Mo white cast irons: The effects of chemical composition and microstructure. *Wear* **2022**, *492–493*, 204208. [[CrossRef](#)]
46. Ramadas, H.; Sarkar, S.; Nath, A.K. Three-body dry abrasive wear properties of 15–5 precipitation hardening stainless steel produced by laser powder bed fusion process. *Wear* **2021**, *470–471*, 203623. [[CrossRef](#)]
47. Damião, C.A.; Alcarria, G.C.; Teles, V.C.; de Mello, J.D.B.; da Silva, W.M. Influence of metallurgical texture on the abrasive wear of hot-rolled wear resistant carbon steels. *Wear* **2019**, *426–427*, 101–111. [[CrossRef](#)]
48. Zafar, S.; Sharma, A.K. Abrasive and erosive wear behaviour of nanometric WC–12Co microwave clads. *Wear* **2016**, *346–347*, 29–45. [[CrossRef](#)]
49. Jian, Y.; Huang, Z.; Xing, J.; Li, J. Effects of chromium additions on the three-body abrasive wear behavior of Fe-3.0 wt% B alloy. *Wear* **2017**, *378–379*, 165–173. [[CrossRef](#)]
50. Hernandez, S.; Hardell, J.; Winkelmann, H.; Ripoll, M.R.; Prakash, B. Influence of temperature on abrasive wear of boron steel and hot forming tool steels. *Wear* **2015**, *338–339*, 27–35. [[CrossRef](#)]
51. Petrica, M.; Katsich, C.; Badisch, E.; Kremsner, F. Study of abrasive wear phenomena in dry and slurry 3-body conditions. *Tribol. Int.* **2013**, *64*, 196–203. [[CrossRef](#)]
52. Delgado, I.R.; Handschuh, M.J. Preliminary Assessment of Seals for Dust Mitigation of Mechanical Components for Lunar Surface Systems. In Proceedings of the 40th Aerospace Mechanisms Symposium, Cocoa Beach, FL, USA, 12–14 May 2010.

53. Budinski, K.G. Adhesive transfer to abrasive particles in abrasion testing. *Wear* **2011**, *271*, 1258–1263. [CrossRef]
54. Fildes, J.M.; Meyers, S.J.; Mulligan, C.P.; Kilaparti, R. Evaluation of the wear and abrasion resistance of hard coatings by ball-on-three-disk test methods—A case study. *Wear* **2013**, *302*, 1040–1049. [CrossRef]
55. Thakare, M.R.; Wharton, J.A.; Wood, R.J.K.; Menger, C. Effect of abrasive particle size and the influence of microstructure on the wear mechanisms in wear-resistant materials. *Wear* **2012**, *276–277*, 16–28. [CrossRef]
56. Nieto, A.; Yang, H.; Jiang, L.; Schoenung, J.M. Reinforcement size effects on the abrasive wear of boron carbide reinforced aluminum composites. *Wear* **2017**, *390–391*, 228–235. [CrossRef]
57. Woldman, M.; van der Heide, E.; Schipper, D.J.; Tinga, T.; Masen, M.A. Investigating the influence of sand particle properties on abrasive wear behaviour. *Wear* **2012**, *294–295*, 419–426. [CrossRef]
58. Qin, K.; Zhou, Q.; Zhang, K.; Feng, Y.; Zhang, T.; Zheng, G.; Xia, B.; Liu, B. Non-uniform abrasive particle size effects on friction characteristics of FKM O-ring seals under three-body abrasion. *Tribol. Int.* **2019**, *136*, 216–223. [CrossRef]
59. Grandy, D.; Panek, N.; Routhier, G.; Ridolfi, P. Development and Qualification of The Exomars Bogie Electro-Mechanical Assembly (Bema) Rotary Actuators. In Proceedings of the ESMATS—18th European Space Mechanisms and Tribology Symposium, Munich, Germany, 18–20 September 2019.
60. Dougherty, S. Micro-Imager Dust Cover, Micro-Imager Contact Sensor, and Mössbauer Spectrometer Contact Sensor Mechanisms for the Mars Exploration Rovers. In European Space Agency, (Special Publication) ESA SP, 2003. Available online: <https://ui.adsabs.harvard.edu/abs/2003ESASP.524...73D/abstract> (accessed on 8 June 2023).
61. Jandura, L. Mars Science Laboratory Sample Acquisition, Sample Processing and Handling: Subsystem Design and Test Challenges. In Proceedings of the 40th Aerospace Mechanisms Symposium, Cocoa Beach, FL, USA, 12–14 May 2010.
62. Ng, T.C.; Yung, K.L. Mars Rock Corer and Planetary Micro Sampling Tools. In Proceedings of the 33rd Lunar and Planetary Science Conference, Houston, TX, USA, 11–15 March 2010.
63. Arkwright, B.; Buchele, P.; Di Leonardo, P. Development of a modular two-axis gimbal mechanism for spacecraft antenna and thruster pointing. In Proceedings of the 8th European Space Mechanisms and Tribology Symposium, Toulouse, France, 29 September–1 October 1999.
64. Description Of Harmonic Gear Assembly Operation Harmonic Drive LLC Web Site. Available online: <http://harmonic-drive.com/> (accessed on 11 October 2022).
65. McClendon, M. NIRSpec MSS Magnet Actuator Life Test Unit Wear Particle Evaluation. 16 May 2011. Available online: <https://esmats.eu/amspapers/pastpapers/pdfs/2012/krantz.pdf> (accessed on 11 October 2022).
66. Galary, J. Rolling Wear and Fatigue in Lubricated Contacts. Ph.D. Thesis, University of Massachusetts at Dartmouth, Dartmouth, MA, USA, 2018.
67. Lamotte, E.; Bozet, J.-L.; Kabuya, A. Modelling of Friction and Wear for Cryogenic Valve Seals of Rocket Engines. Techspace Aero, 2000. Available online: <https://www.esmats.eu/esmatspapers/pastpapers/pdfs/1999/lamotte.pdf> (accessed on 11 October 2022).
68. Provedo, B.; Jaio, G.; Viñals, J. Sealing cap for metis instrument in solar orbiter fdm subsystem. In *ESMATS 2017*; SENER: Getxo, Spain, 2017; pp. 20–22.
69. Sidz, M.; Poweska, Ł.; Wilson, N.; Pulker, S. Umbilical Release Mechanisms (URM) for exomars2020 mission. In Proceedings of the European Space Mechanisms and Tribology Symposium, Munich, Germany, 18–20 September 2019; pp. 18–20.
70. Fouché, F.; Leproux, F.; Leverd, M.; Sicre, J. Development and Qualification of a High-Temperature Shape Memory Alloys Based Actuator for Hold Down and Release Mechanisms (HDRM). 19th ESMATS, 2021. Available online: <https://www.esmats.eu/esmatspapers/pastpapers/pdfs/2021/fouche2.pdf> (accessed on 11 October 2022).
71. Poweska, Ł.; Sidz, M.; Ybarra, G. Qualification of Resource Transfer Mechanisms as Part of International Berthing and Docking Mechanism—Hard Capture System Development. 19th ESMATS, 2021. Available online: <https://www.esmats.eu/esmatspapers/pastpapers/pdfs/2021/poweska.pdf> (accessed on 11 October 2022).
72. Obara, S.; Sasaki, A.; Haraguchi, M.; Imagawa, K.; Nishimura, M.; Kawashima, N. Evaluation tests of industrial vacuum bearings for space use. *Tribotest* **2003**, *10*, 117–134. [CrossRef]
73. Schmalbach, M.; Eigenmann, M.; Schmidt, T. Development of a Two Hinge Shutter and Calibration Mechanism. 2011. Available online: www.enmap.com (accessed on 8 June 2023).
74. Verhoeven, D.; Renté, D. Locking mechanism for ixv re-entry demonstrator flap control system. In Proceedings of the 14th European Space Mechanisms and Tribology Symposium—ASMATS, Constance, Germany, 28–30 September 2011.
75. Viñals, J.; Borque, C.; Jaio, G.; Provedo, B. Doors mechanism for feedthrough operation in solar orbiter FDM subsystem. In Proceedings of the 16th European Space Mechanisms and Tribology Symposium 2015, Bilbao, Spain, 1–30 September 2015.
76. Garland, M.; Allouis, E.; Rucinski, M.; Coates, A.; Marc, R. Design and Implementation of the Lightweight Advanced Robotic Arm Demonstrator (LARAD). 2017. Available online: <https://www.esmats.eu/esmatspapers/pastpapers/pdfs/2017/garland.pdf> (accessed on 14 October 2022).
77. Strube, B.; Glier, M.; Manthey, K.; Trauthan, F.; Schmitz, N.; Jaumann, R.; Michaelis, H. Exomars Pancam High Resolution Camera (HRC): Evolution from BB to FM. 2019. Available online: <https://esmats.eu/esmatspapers/pastpapers/pdfs/2019/strube2.pdf> (accessed on 7 November 2022).
78. Jones, W.R.; Jansen, M.J.; Gschwender, L.J.; Snyder, C.E.; Sharma, S.K.; Predmore, R.E.; Dube, M.J. The tribological properties of several silahydrocarbons for use in space mechanisms. *J. Synth. Lubr.* **2004**, *20*, 303–315. [CrossRef]

79. Cadiergues, L.; Bourdit, C.; Trouchet, D.; Larcher, V.; Sugranes, P.; Leletty, R. A mirror control mechanism for space telescope. In Proceedings of the 10th European Space Mechanisms and Tribology Symposium, San Sebastián, Spain, 24–26 September 2003.
80. Henein, S.; Spanoudakis, P.; Schwab, P.; Giriens, L.; Lisowski, L.; Onillon, E.; Myklebust, L.I. Mechanical slit mask mechanism for the James Webb Space Telescope spectrometer. In *Optical, Infrared, and Millimeter Space Telescopes*; SPIE: Bellingham, WA, USA, 2003.
81. Caprini, G.C.; Mondello, G.; Brotini, M.; Corsini, R.; Gasparini, L.; Battazza, F.; Formaro, R. Main port mechanism for Prisma. In Proceedings of the 15th European Space Mechanisms and Tribology Symposium (ESMATS), Noordwijk, The Netherlands, 25–27 September 2013.
82. Mohtar, T.; Bursi, A.; Galbiati, A.; Spinelli, M. Actuated Cover Door with Emergency Opening Function for Space Telescopes. 19th ESMATS, 2021. Available online: <https://www.esmats.eu/esmatspapers/pastpapers/pdfs/2021/mohtar.pdf> (accessed on 15 October 2022).
83. Nava, N.; Collado, M.; Cabás, R. New deployment mechanisms based on SMA technology for space applications. In Proceedings of the 15th European Space Mechanisms and Tribology Symposium (ESMATS), Noordwijk, The Netherlands, 25–27 September 2013.
84. Thiel, M.; Stöcker, J.; Rohe, C.; Kömle, N.I.; Kargl, G.; Hillenmaier, O.; Lell, P. The Rosetta lander anchoring system. In Proceedings of the 10th European Space Mechanisms and Tribology Symposium, San Sebastián, Spain, 25 September 2003.
85. Billing, R. Caging Mechanisms for the Mars Exploration Rover Instrument Deployment Device. 2003. Available online: <http://www.asi-space.com> (accessed on 8 June 2023).
86. Billing, P.A.R.; Fleischner, C.-A.R. Mars Science Laboratory Robotic Arm. In Proceedings of the 14th European Space Mechanisms and Tribology Symposium—ASMATS, Constance, Germany, 28–30 September 2011.
87. Urgoiti, E.; Ramirez, A.; Coste, P. GAIA M2M positioning mechanism. In Proceedings of the 11th Euro. Space Mechanisms & Tribology Symp (ESMATS), Lucerne, Switzerland, 21–23 September 2005.
88. Campo, P.; Barrio, A.; Puente, N.; Kyle, R. Development of a high temperature antenna pointing mechanisms for Bepicolombo planetary orbiter. In Proceedings of the 15th European Space Mechanisms and Tribology Symposium (ESMATS), Noordwijk, The Netherlands, 25–27 September 2013.
89. Gewehr, M.; Schneider, A.; Dalcolmo, J.; Klinkner, S.; GmbH, S. Design and Testing of a Novel Miniaturised Sealed Tether-Recoil Mechanism for the Nanokhod Micro rover. ESMATS, 2021. Available online: <https://esmats.eu/esmatspapers/pastpapers/pdfs/2021/gewehr.pdf> (accessed on 15 October 2022).
90. Schmid, B.; Flüeli, P.; Houghton, P.; Blum, D. Development of the lid opening mechanism (LOM). In Proceedings of the 13th European Space Mechanisms & Tribology Symposium, Vienna, Austria, 23–25 September 2009.
91. Melzer, C.; Cubillo, A.A.; Nadler, M.; Pfitzner, F.; Hahn, R. Mechanical Testing on the Core Sample Transportation Mechanism of the ExoMars 2018 Mission. Available online: <https://esmats.eu/esmatspapers/pastpapers/pdfs/2015/melzer.pdf> (accessed on 7 November 2022).
92. Paul, R.; Tattusch, T.; Redlich, D.; Ott, S.; Dobrea, D.; Richter, L.; Thiel, M.; Cubillo, A.; Weisz, H.; Musso, F.; et al. ‘Backlash-free’ gas-tight high precision sample handling mechanisms – lessons learned from qualification testing & Design and lessons learned of the core sample handling mechanism (cshs) on the ExoMars 2020 rover. In Proceedings of the 43rd Aerospace Mechanisms Symposium, NASA Ames Research Center, Hatfield, UK, 20–22 September 2017.
93. Suetta, E.; Cherubini, G.; Mondello, G.; Piccini, G. Four Cover Mechanisms for the Rosetta Mission. Available online: <https://ui.adsabs.harvard.edu/abs/1999ESASP.438..127S/abstract> (accessed on 8 June 2023).
94. Kiener, L.; Perruchoud, G.; Schwab, P.; Verhaeghe, A.; Spanoudakis, P.; Gumy, M. Development challenges of a focus mechanism for EXOMARS mission submitted to the harsh Martian environment. In *Advances in Optical and Mechanical Technologies for Telescopes and Instrumentation*; SPIE: Bellingham, WA, USA, 2018; p. 39. [CrossRef]
95. Tattusch, T.; Wieser, J.; Müller, A.; Mecucci, C.B.; Senese, S.; Böhm, V.; Jalba, L.; Schwarz, C. DEAR-Providing a Dusty Environment for Planetary Exploration Robotics Testing. 19th ESMATS, 2021. Available online: <https://esmats.eu/esmatspapers/pastpapers/pdfs/2021/tattusch.pdf> (accessed on 15 October 2022).
96. Budzyn, D.; Zare-Behtash, H.; Cowley, A.; Cammarano, A. Topology optimization of compliant mechanisms as a design method to improve hardware performance in lunar dust environment. In Proceedings of the 19th European Space Mechanisms and Tribology Symposium, Online, 20–24 September 2021.
97. Baumgartner, E.T.; Bonitz, R.G.; Melko, J.P.; Shiraiishi, L.R.; Leger, P.C. The Mars Exploration Rover Instrument Positioning System. 2005 IEEE Aerospace Conference, 2005. Available online: https://www.academia.edu/4453248/The_Mars_Exploration_Rover_instrument_positioning_system (accessed on 7 June 2023).
98. Harrington, B.D.; Voorhees, C. The Challenges of Designing the Rocker-Bogie Suspension for the Mars Exploration Rover. In Proceedings of the 37th Aerospace Mechanisms Symposium, Galveston, TX, USA, 29–21 May 2004.
99. Colorado School of Mines, Planetary Simulant Database. Available online: <https://simulantdatab.com/> (accessed on 11 July 2023).
100. Chuang, K.C.; Gornet, T.J.; Schneidau, K.; Koerner, H. Laser Sintering of Thermoset Polyimide Composites 2019. Available online: <https://ntrs.nasa.gov/search.jsp?R=20190031841> (accessed on 15 October 2022).

Disclaimer/Publisher’s Note: The statements, opinions and data contained in all publications are solely those of the individual author(s) and contributor(s) and not of MDPI and/or the editor(s). MDPI and/or the editor(s) disclaim responsibility for any injury to people or property resulting from any ideas, methods, instructions or products referred to in the content.